1 December 2000

ELSEVIER

Optics Communications 186 (2000) 185–209

OPTICS COMMUNICATIONS

www.elsevier.com/locate/optcom

Diffraction effects in the self-amplified spontaneous emission FEL

E.L. Saldin [a,*], E.A. Schneidmiller [a], M.V. Yurkov [b]

[a] *Deutches Elektronen Synchrotron (DESY), HASYLAB, Building 25F, Room 452, Notkestrasse 85, 22607 Hamburg, Germany*
[b] *Joint Institute for Nuclear Research, Dubna 141980, Moscow Region, Russian Federation*

Received 20 June 2000; received in revised form 16 October 2000; accepted 16 October 2000

Abstract

In this paper we present a systematic approach for analytical description of SASE FEL (SASE: self-amplified spontaneous emission) in the linear mode. We calculate the average radiation power, radiation spectrum envelope, angular distribution of the radiation intensity in far zone, longitudinal and transverse correlation functions, degree of transverse coherence etc. Using the results of analytical calculations presented in reduced form, we analyze various features of the SASE FEL in the linear mode. The general result is applied to the special case of an electron beam having Gaussian profile and Gaussian energy distribution. These analytical results can serve as a primary standard for testing the codes. In this paper we present numerical study of the process of amplification in the SASE FEL using three-dimension time-dependent code FAST. Comparison with analytical results shows that in the high-gain linear limit there is good agreement between the numerical and analytical results. It has been found that even after finishing the transverse mode selection process the degree of transverse coherence of the radiation from SASE FEL visibly differs from unity. This is consequence of the interdependence of the longitudinal and transverse coherence. The SASE FEL has poor longitudinal coherence which develops slowly with the undulator length thus preventing a full transverse coherence. © 2000 Elsevier Science B.V. All rights reserved.

Keywords: Free electron laser; High-gain FEL; Initial-value problem; Coherence

1. Introduction

Fluctuations of the electron beam current density can serve as the input signal in the FEL amplifier. These fluctuations always exist in the electron beam due to the effect of shot noise. An FEL amplifier which starts up from shot noise is frequently known as self-amplified spontaneous emission (SASE) FEL.

A complete description of the SASE FEL can be performed only with three-dimensional (3-D) time-dependent numerical simulation codes. Application of the numerical calculations allows one to describe the general case of the SASE FEL operation, including the case of an arbitrary axial and transverse profile

* Corresponding author. Tel.: +49-40-8998-2676; fax: +49-40-8998-4705.
E-mail address: saldin@mail.desy.de (E.L. Saldin).

0030-4018/00/$ - see front matter © 2000 Elsevier Science B.V. All rights reserved.
PII: S0030-4018(00)01061-0

of the electron bunch, the effects of finite pulse duration and nonlinear effects. Since construction of the 3-D time-dependent codes is a rather complicated problem, significant attention should be devoted to testing the codes. On the other hand, testing the numerical simulation codes would be difficult without the use of analytical results of SASE FEL linear theory as a primary standard. With the design and construction of VUV and X-ray FELs, many 3-D time-dependent codes (GINGER [1], GENESIS [2], FAST [3]) have been developed over the years in order to describe FEL amplifier start-up from shot noise. Nevertheless, it should be emphasized that despite these codes are widely used in the design of X-ray FELs [4–7], there are no comparison between numerical simulation and analytical results of 3-D SASE FEL theory.

In this paper we present a systematic approach for calculations of the average radiation power, radiation spectrum envelope, and angular distribution of the radiation intensity in the far zone, and degree of transverse coherence. These analytical results serve as a primary standard for testing the codes. Numerical simulations have been performed with 3-D time-dependent code FAST [3]. Comparison with analytical results shows that in the high-gain linear limit there is a good agreement between the numerical and analytical results.

From the theoretical point of view the SASE FEL, is a rather complicated object, so it is important to find a model which provides the possibility of an analytical description without loss of essential information about the features of the SASE process. When deriving analytical results we used the model of a long electron bunch with rectangular axial profile of the current. Investigation of the SASE FEL process is performed with steady-state spectral Green's function connecting the Fourier amplitudes of the output field and the Fourier amplitudes of the input noise signal. Since in the linear regime all the harmonics are amplified independently, we can use the result of steady-state theory for each harmonic and calculate the corresponding Fourier harmonics of output radiation field. In the framework of this model it becomes possible to describe analytically all the statistical properties of the radiation from the SASE FEL.

Some averaged output characteristics of SASE FEL in framework of one-dimensional (1-D) model have been obtained in Refs. [8,9]. An approach for 1-D time-dependent numerical simulations of SASE FEL have been developed in Refs. [10,11]. Realization of this approach allowed to obtain some statistical properties of radiation from a SASE FEL operation in linear and nonlinear regime [12,13]. A comprehensive study of the statistical properties of the radiation from the SASE FEL in framework of the same model is presented in Ref. [14]. The accuracy of these numerical results is controlled by means of analytical results of 1-D SASE FEL theory.

The 3-D theory of the SASE FEL is more complicated than that of the simplified 1-D model. The actual physical picture of start-up from noise should take into account that the fluctuations of the current density in the electron beam are uncorrelated not only in time but in space too. Thus a large number of transverse radiation modes are excited when the electron beam enters the undulator. These radiation modes have different growth rates. During the amplification process, the number of transverse modes decreases. Also, the divergence of radiation beam in far zone decreases. For a sufficiently long undulator the fundamental mode, which has maximal gain, should survive. Information on transverse coherence formation can be obtained with analytical solution of initial value problem.

When the FEL amplifier operates in the steady-state linear regime, the driving electron beam can be considered as an active medium whose properties do not depend on the longitudinal coordinate z. Let us analyze the nature of the self-consistent solution of Maxwell's equations and the Vlasov equation at a fixed frequency ω. The electric field of the wave radiated in the helical undulator may be represented in the complex form:

$$E_x + \mathrm{i}E_y = \widetilde{E}(z, \vec{r}_\perp) \exp[\mathrm{i}\omega(z/c - t)]. \tag{1}$$

At a sufficient distance from the undulator entrance the radiation can be presented as a superposition of the exponentially growing guided modes

$$\widetilde{E}(z,\vec{r}_\perp) = \sum_j A_j \Phi_j(\vec{r}_\perp) \exp(\Lambda_j z),$$

where Λ_j and $\Phi_j(\vec{r}_\perp)$ are the eigenvalues and the eigenfunctions of the guiding modes, respectively, and $\mathrm{Re}(\Lambda_j) > 0$. The rigorous solution of the eigenvalue problem for an axisymmetric electron beam with stepped profile was obtained in Ref. [15]. The model of the FEL amplifier considered in that paper is based on a full 3-D description of electromagnetic field, but the electron motion is considered to be one dimensional. Later the initial-value problem was solved in Ref. [16] in framework of the same model of the electron beam.

An effect similar to the optical guiding effects occurs in optical fibers. However, unlike guided modes in fiber optics, FEL guided modes are not orthogonal. To solve the initial-value problem in the case of arbitrary gradient beam profile, approaches other than direct mode expansion must be used. The first step in this direction was taken by Kim [17], who has applied a method of solution, originally introduced by van Kampen [18]. A Laplace transform method was employed by Krinsky and Yu [19], leading to a Green's function. This Green's function can still be expanded in terms of orthonormal eigenfunctions of the associated two-dimensional (2-D) Schrödinger equation with non-self-adjoint Hamiltonian. In the high-gain limit, the asymptotic representation of the Green's function is found to be dominated by the contribution of the guided modes.

The eigenvalue problem for the case of an arbitrary gradient axisymmetric profile is solved by means of the multilayer approximation method [20]. Based on these solutions, complete information on the eigenfunctions and eigenvalues can be extracted, and used, for calculations of the output radiation field. General solution for Green's function [19] gives us input coupling factors A_j. As a result we are able to calculate the average radiation power, radiation spectrum envelope, angular distribution of the radiation intensity in far zone, and degree of transverse coherence.

The paper is organized as follows. In Section 2 we discuss the coupled Vlasov–Maxwell equations, and for the case of an electron beam with energy spread, we derive a partial integro-differential equation describing the evolution of the radiation field. In high-gain regime the output radiation is expressed in terms of exponentially growing guiding modes. We analyze the FEL amplifier with an arbitrary gradient profile. Such an analysis of guided modes is performed with the multilayer approximation method [20]. The radiated field is determined with use of the Green's function [19]. This systematic approach allows one to perform a complete description of the FEL amplifier with an arbitrary gradient profile of the electron beam. It is shown that this formalism is easily generalized to allow the inclusion of space charge effects. Theoretical study is performed with an extensive use of similarity techniques. In Section 3 we derive analytical expressions for the average output radiation power, spectrum and angular distribution of the radiation intensity in the far zone for the SASE FEL. In Section 4 we describe general features of the algorithm for time-dependent simulations implemented in the code FAST [3]. In Section 5 we present specific numerical example of the SASE FEL operating in the linear regime calculated with analytical formulae and numerical simulation code. It is shown that there is good agreement of the analytical and numerical results in the high-gain regime. In Sections 6 and 7 we analyze the process of formation of transverse coherence in the SASE FEL. It is shown that even after finishing the transverse mode selection process the degree of transverse coherence of the radiation from SASE FEL visibly differs from unity. This is consequence of the interdependence of the longitudinal and transverse coherence. The SASE FEL has poor longitudinal coherence which develops slowly with the undulator length thus preventing a full transverse coherence.

2. Analytical description of the steady-state linear regime

2.1. Self-consistent equation

Let us consider electron beam moving along the z axis in the field of a helical undulator. The magnetic field of the undulator may be written in the complex form:

$$H_x + \mathrm{i}H_y = H_\mathrm{w} \exp(-\mathrm{i}k_\mathrm{w} z).$$

We neglect the transverse variation of the undulator field and assume the electrons move along constrained helical trajectories in parallel with the z axis. The electron rotation angle is considered to be small and the longitudinal electron velocity v_z is close to the velocity of light c. We describe the electron motion using energy-phase variables $P = \mathscr{E} - \mathscr{E}_0$ and $\psi = k_\mathrm{w} z + \omega(z/c - t)$, where $\mathscr{E}$ is the kinetic energy of the electron, $\mathscr{E}_0$ is the nominal energy. The evolution of the distribution function of the electron beam $f(P, \psi, z)$ is governed by the Vlasov equation

$$\frac{\partial f}{\partial z} + \frac{\partial H}{\partial P}\frac{\partial f}{\partial \psi} - \frac{\partial H}{\partial \psi}\frac{\partial f}{\partial P} = 0, \tag{2}$$

where

$$H = CP + \frac{\omega}{2c\gamma_z^2 \mathscr{E}_0} P^2 - (U\mathrm{e}^{\mathrm{i}\psi} + U^*\mathrm{e}^{-\mathrm{i}\psi}) + e\int \mathrm{d}\psi E_z \tag{3}$$

is effective Hamiltonian, $C = k_\mathrm{w} - \omega/(2c\gamma_z^2)$ is the detuning of the electron with the nominal energy $\mathscr{E}_0$, $U = -e\theta_\mathrm{s}\widetilde{E}(z, \vec{r}_\perp)/(2\mathrm{i})$ is the complex amplitude of the effective potential of the particle interaction with the electromagnetic wave, $(-e)$ is the charge of electron, $E_z(\psi, z, \vec{r}_\perp)$ is the longitudinal space charge field,

$$\theta_\mathrm{s} = eH_\mathrm{w}/(\mathscr{E}_0 k_\mathrm{w}) = K/\gamma$$

is the rotation angle of the electron with nominal energy,

$$\gamma_z^{-2} = \gamma^{-2} + \theta_\mathrm{s}^2, \quad \gamma = \mathscr{E}_0/(m_\mathrm{e}c^2),$$

and m_e is the rest mass of electron. It should be noted that the radiation field and the space charge field depend on the transverse coordinate $\vec{r}_\perp$. So, in the present consideration these fields are three dimensional. At the same time, the dynamical equations corresponding to the effective Hamiltonian (3) are one dimensional. This means that from the point of view of dynamics the transverse coordinate $\vec{r}_\perp$ is a parameter, but not a dynamical variable.

We solve Eq. (2) using the perturbation method. For an electron beam with a small density perturbation we seek solutions for f and E_z in the form

$$f = f_0 + \tilde{f}_1\mathrm{e}^{\mathrm{i}\psi} + \tilde{f}_1^*\mathrm{e}^{-\mathrm{i}\psi}, \qquad E_z = \widetilde{E}_z\mathrm{e}^{\mathrm{i}\psi} + \widetilde{E}_z^*\mathrm{e}^{-\mathrm{i}\psi}.$$

Here $f_0(\vec{r}_\perp, P)$ is the unperturbed distribution function and $\widetilde{f_1}(\vec{r}_\perp, P, z)$ is the small perturbation. In the linear approximation we get

$$\frac{\partial \tilde{f}_1}{\partial z} + \mathrm{i}\left[C + \omega P/(c\gamma_z^2 \mathscr{E}_0)\right]\tilde{f}_1 + \left(\mathrm{i}U - e\widetilde{E}_z\right)\frac{\partial f_0}{\partial P} = 0. \tag{4}$$

We assume that

$$f_0 = n_0 F(P), \quad \int F(P)\,\mathrm{d}P = 1,$$

where n_0 is the beam density. The solution of Eq. (4) has the form

$$\tilde{f}_1 = -n_0 \frac{\mathrm{d}F}{\mathrm{d}P} \int_0^z \mathrm{d}z' (\mathrm{i}U - e\widetilde{E}_z) \exp\left\{\mathrm{i}\left[C + \omega P/(c\gamma_z^2 \mathscr{E}_0)\right](z' - z)\right\} + \tilde{f}_1|_{z=0} \exp\{-\mathrm{i}[C + \omega P/(c\gamma_z^2 \mathscr{E}_0)]z\}. \tag{5}$$

In the ultrarelativistic approximation $v_z \simeq c$, so the beam current density and the distribution function are related as

$$j_z = -j_0(\vec{r}_\perp) + \tilde{j}_1 \mathrm{e}^{\mathrm{i}\psi} + \text{c.c.}, \quad \tilde{j}_1 \simeq -ec \int \tilde{f}_1 \, \mathrm{d}P,$$

where $-j_0(\vec{r}_\perp) \simeq -ecn_0(\vec{r}_\perp)$ is the longitudinal component of the unperturbed beam current density. The minus sign appears in the expression because electrons have charge $(-e)$ and move in the positive direction of the z axis.

In what follows we assume that the transverse size of the electron beam is large, i.e. $r_\mathrm{b}^2 \gg \gamma_z^2 c^2/\omega^2$. In the framework of the accepted limitation on the transverse size of the electron beam we can derive from Maxwell's equations the following expression for the longitudinal space charge field:

$$\widetilde{E}_z = -\mathrm{i}\frac{4\pi}{\omega}\tilde{j}_1(z, \vec{r}_\perp). \tag{6}$$

In this paper we consider the specific, but important practical case of the following initial conditions – the electron beam is modulated only in density at the undulator entrance $\tilde{f}_1|_{z=0} = a_\mathrm{ext}(\vec{r}_\perp)F(P)$ – the field amplitude of the electromagnetic wave $\widetilde{E}$ takes the value $\widetilde{E}|_{z=0} = 0$ at the undulator entrance. Substituting Eq. (6) into Eq. (5), integrating over P and using specific initial condition at the undulator entrance, we obtain the following integral equation for $\tilde{j}_1$:

$$\tilde{j}_1 = \mathrm{i}j_0(\vec{r}_\perp) \int_0^z \mathrm{d}z' [U + 4\pi e\tilde{j}_1/\omega] \int_{-\infty}^{\infty} \mathrm{d}P \frac{\mathrm{d}F(P)}{\mathrm{d}P} \exp\left\{\mathrm{i}\left[C + \omega P/(c\gamma_z^2 \mathscr{E}_0)\right](z' - z)\right\} + a_\mathrm{ext}(\vec{r}_\perp)$$
$$\times \int_{-\infty}^{\infty} \mathrm{d}P F(P) \exp\{-\mathrm{i}[C + \omega P/(c\gamma_z^2 \mathscr{E}_0)]z\}. \tag{7}$$

One more relation, connecting the field and the current density, should come from the solution of the electrodynamic problem. We solve the electrodynamic problem using the paraxial approximation. In this case the wave equation may be written in the following form:

$$c^2[\nabla_\perp^2 + 2\mathrm{i}(\omega/c)\partial/\partial z]\widetilde{E} = -4\pi\mathrm{i}\theta_\mathrm{s}\omega\tilde{j}_1, \tag{8}$$

where $\nabla_\perp^2$ is the Laplace operator in transverse coordinates. This equation has been derived using the assumption that the complex amplitudes, $\tilde{j}_1$ and $\widetilde{E}$, are slowly varying functions on the scale of the undulator period.

So, we have obtained the system of self-consistent field equations (7) and (8). Let us consider an axisymmetric electron beam with gradient profile of the current density. When considering axisymmetric systems, it is convenient to rewrite Eqs. (7) and (8) using cylindrical coordinates (r, φ, z). The general form of the transverse distribution of the beam current density of axisymmetric electron beam is

$$j_0(r) = I_0 S(r/r_0) \left[2\pi \int_0^\infty rS(r/r_0)\,\mathrm{d}r\right]^{-1}, \tag{9}$$

where r_0 is the beam profile parameter (typical transverse size of the beam) and I_0 is the beam current. To be specific, we set $S(0) = 1$. We represent $\widetilde{E}$ and $\tilde{j}_1$ as a Fourier series in the angle φ:

$$\widetilde{E}(z, r, \varphi) = \sum_{n=-\infty}^{n=+\infty} \widetilde{E}^{(n)}(z, r)\mathrm{e}^{-\mathrm{i}n\varphi}, \qquad \tilde{j}_1(z, r, \varphi) = \sum_{n=-\infty}^{n=+\infty} \tilde{j}_1^{(n)}(z, r)\mathrm{e}^{-\mathrm{i}n\varphi}.$$

Substituting Eq. (7) into right-hand side of Eq. (8), we obtain a single integro-differential equation for the field amplitude $\widetilde{E}^{(n)}$. It is convenient to write this equation in the following dimensionless form:

$$\left[\frac{\partial^2}{\partial\hat{r}^2}+\frac{1}{\hat{r}}\frac{\partial}{\partial\hat{r}}-\frac{n^2}{\hat{r}^2}+2\mathrm{i}B\frac{\partial}{\partial\hat{z}}\right]\hat{E}^{(n)}(\hat{z},\hat{r})=\mathrm{i}S(\hat{r})\int_0^{\hat{z}}\mathrm{d}\hat{z}'\left\{2+\hat{\Lambda}_{\mathrm{p}}^2\left[\frac{\partial^2}{\partial\hat{r}^2}+\frac{1}{\hat{r}}\frac{\partial}{\partial\hat{r}}-\frac{n^2}{\hat{r}^2}+2\mathrm{i}B\frac{\partial}{\partial\hat{z}'}\right]\right\}\hat{E}^{(n)}(\hat{z}',\hat{r})$$
$$\times\int_{-\infty}^{\infty}\mathrm{d}\hat{P}\,\mathrm{d}\hat{F}(\hat{P})/\mathrm{d}\hat{P}\,\exp[\mathrm{i}(\hat{P}+\hat{C})(\hat{z}'-\hat{z})]+4\mathrm{i}\hat{a}_{\mathrm{ext}}^{(n)}(\hat{r})S(\hat{r})$$
$$\times\int_{-\infty}^{\infty}\mathrm{d}\hat{P}\hat{F}(\hat{P})\,\exp[-\mathrm{i}(\hat{P}+\hat{C})\hat{z}]. \tag{10}$$

Here the following notation is introduced: $\hat{z}=\Gamma z$, $\hat{r}=r/r_0$, $\hat{C}=C/\Gamma$ is the detuning parameter, $B=r_0^2\Gamma\omega/c$ is the diffraction parameter,

$$\hat{\Lambda}_{\mathrm{p}}^2=\Lambda_{\mathrm{p}}^2/\Gamma^2=4c^2(\theta_{\mathrm{s}}r_0\omega)^{-2}$$

is the space charge parameter,

$$\Gamma=\left[I_0\omega^2\theta_{\mathrm{s}}^2\left(2I_{\mathrm{A}}c^2\gamma_z^2\gamma\int_0^{\infty}\zeta S(\zeta)\,\mathrm{d}\zeta\right)^{-1}\right]^{1/2}$$

is the gain parameter, $I_{\mathrm{A}}\simeq 17$ kA is the Alfven current. The complex amplitudes $\widetilde{E}^{(n)}$ and $\hat{E}^{(n)}$ are connected by the relation

$$\hat{E}^{(n)}=\widetilde{E}^{(n)}/E_0,\quad E_0=\rho\mathscr{E}_0\Gamma/(e\theta_{\mathrm{s}}),$$

where $\rho=c\gamma_z^2\Gamma/\omega$ is the efficiency parameter. The complex amplitude of the first harmonic of the beam current density $\tilde{j}_1^{(n)}$ is connected with $\hat{a}_1^{(n)}$ by the relation

$$\hat{a}_1^{(n)}(\hat{z},\hat{r})=-\tilde{j}_1^{(n)}(\hat{z},\hat{r})/j_0(\hat{r}),\quad \hat{a}_{\mathrm{ext}}^{(n)}(\hat{r})=\hat{a}_1^{(n)}(\hat{z},\hat{r})|_{z=0}.$$

The energy deviation is normalized as

$$\hat{P}=(\mathscr{E}-\mathscr{E}_0)/(\rho\mathscr{E}_0),$$

and the distribution function for the normalized energy deviation, $\hat{F}(\hat{P})$, is normalized to unity:

$$\int_{-\infty}^{\infty}\hat{F}(\hat{P})\,\mathrm{d}\hat{P}=1.$$

When the energy spread in the electron beam is Gaussian

$$F(\mathscr{E}-\mathscr{E}_0)=(2\pi\langle(\Delta\mathscr{E})^2\rangle)^{-1/2}\exp\left(-\frac{(\mathscr{E}-\mathscr{E}_0)^2}{2\langle(\Delta\mathscr{E})^2\rangle}\right),$$

the corresponding normalized distribution has the form:

$$\hat{F}(\hat{P})=(2\pi\hat{\Lambda}_T^2)^{-1/2}\exp\left(-\frac{\hat{P}^2}{2\hat{\Lambda}_T^2}\right).$$

The energy spread parameter, $\hat{\Lambda}_T^2$, is related to the rms energy spread, $\langle(\Delta\mathscr{E})^2\rangle$, as

$$\hat{\Lambda}_T^2=\langle(\Delta\mathscr{E})^2\rangle/(\rho^2\mathscr{E}_0^2).$$

2.2. Solution of the initial-value problem by the Laplace technique

Eq. (10) is an integro-differential equation for the field amplitude $\hat{E}^{(n)}$ and can be solved by the Laplace transform technique. We solve Eq. (10) with specific initial conditions at $z = 0$:

- the electron beam is modulated in density at the undulator entrance;
- the field amplitude of the electromagnetic wave $\widetilde{E}$ takes the value $\widetilde{E}|_{z=0} = 0$ at the undulator entrance.

The Laplace transforms of the $\hat{E}^{(n)}$,

$$\bar{E}^{(n)}(p,\hat{r}) = \int_0^\infty \mathrm{e}^{-p\hat{z}}\hat{E}^{(n)}(\hat{z},\hat{r})\,\mathrm{d}\hat{z},$$

satisfy the following equation

$$\left[\frac{\partial^2}{\partial\hat{r}^2} + \frac{1}{\hat{r}}\frac{\partial}{\partial\hat{r}} - \frac{n^2}{\hat{r}^2} + 2\mathrm{i}Bp - \frac{2\mathrm{i}\hat{D}(p)S(\hat{r})}{1 - \mathrm{i}\hat{\Lambda}_\mathrm{p}^2 S(\hat{r})\hat{D}(p)}\right]\bar{E}^{(n)}(p,\hat{r}) = 4\mathrm{i}\hat{a}_\mathrm{ext}^{(n)}(\hat{r})S(\hat{r})\hat{D}_0(p), \tag{11}$$

where

$$\hat{D} = \int_{-\infty}^{\infty}\mathrm{d}\hat{P}\frac{\mathrm{d}\hat{F}(\hat{P})/\mathrm{d}\hat{P}}{p + \mathrm{i}(\hat{P} + \hat{C})}, \qquad \hat{D}_0 = \int_{-\infty}^{\infty}\mathrm{d}\hat{P}\frac{\hat{F}(\hat{P})}{p + \mathrm{i}(\hat{P} + \hat{C})}.$$

So, using the Fourier expansion and the Laplace transform allows us to go over from partial integro-differential equation to the ordinary differential equation. To find $\bar{E}^{(n)}$, one must solve Eq. (11) with the boundary condition

$$\bar{E}^{(n)}(p,\hat{r}) \to 0 \quad \text{for } \hat{r} \to \infty.$$

We rewrite Eq. (11) as

$$\left[\frac{\partial^2}{\partial\hat{r}^2} + \frac{1}{\hat{r}}\frac{\partial}{\partial\hat{r}} - \frac{n^2}{\hat{r}^2} + g(\hat{r},p)\right]\bar{E}^{(n)}(p,\hat{r}) + 2\mathrm{i}Bp\bar{E}^{(n)}(p,\hat{r}) = f^{(n)}(\hat{r},p). \tag{12}$$

Here the following notation is introduced

$$g(\hat{r},p) = -\frac{2\mathrm{i}\hat{D}(p)S(\hat{r})}{1 - \mathrm{i}\hat{\Lambda}_\mathrm{p}^2 S(\hat{r})\hat{D}(p)},$$

$$f^{(n)}(\hat{r},p) = 4\mathrm{i}\hat{a}_\mathrm{ext}^{(n)}(\hat{r})S(\hat{r})\hat{D}_0(p).$$

2.2.1. Green's function

Eq. (11) is nonhomogeneous, linear, second-order differential equation. The homogeneous equation is satisfied by its eigenfunctions $\Phi_{nj}(\hat{r})$,

$$\left[\frac{\partial^2}{\partial\hat{r}^2} + \frac{1}{\hat{r}}\frac{\partial}{\partial\hat{r}} - \frac{n^2}{\hat{r}^2} + g(\hat{r},\lambda_j^{(n)})\right]\Phi_{nj} + 2\mathrm{i}B\lambda_j^{(n)}\Phi_{nj} = 0. \tag{13}$$

Formally this equation is similar to the 2-D Schrödinger's equation with complex potential

$$\left[\frac{\partial^2}{\partial\hat{r}^2}+\frac{1}{\hat{r}}\frac{\partial}{\partial\hat{r}}-\frac{n^2}{\hat{r}^2}+w(\hat{r})\right]\Psi_{nj}+\Lambda_j^{(n)}\Psi_{nj}=0. \tag{14}$$

Nevertheless, there is a principal difference. In Eq. (14) the weight function $w(\hat{r})$ takes the same values for all eigenfunctions, while $g(\hat{r},\lambda_j^{(n)})$ appearing in Eq. (13) depends on the eigenvalue $\lambda_j^{(n)}$. As a result, eigenfunctions of the homogeneous equation (13) are not orthogonal and the eigenfunction expansion of the Green's function does not exist. In this case the analytical solution of the nonhomogeneous equation (11) can be obtained using the following mathematical trick. Let us consider associated eigenvalue problem

$$\left[\frac{\partial^2}{\partial\hat{r}^2}+\frac{1}{\hat{r}}\frac{\partial}{\partial\hat{r}}-\frac{n^2}{\hat{r}^2}+g(\hat{r},p)\right]\Psi_{nj}+\Lambda_j^{(n)}\Psi_{nj}=0. \tag{15}$$

For the present, we assume that $p=$ constant, that associated differential equation is Schrödinger's equation where $\Lambda_j^{(n)}$ is the eigenvalue and $g(\hat{r},p)$ is a known weight function. A function $\Psi_{nj}(\hat{r})$, which satisfies Eq. (15) and the imposed boundary conditions, is called an eigenfunction corresponding to $\Lambda_j^{(n)}$. Taking the complex conjugate of Eq. (15) we obtain $g(\hat{r},p)^*\neq g(\hat{r},p)$. This property is expressed by saying that the operator

$$\mathscr{L}=\frac{\partial^2}{\partial\hat{r}^2}+\frac{1}{\hat{r}}\frac{\partial}{\partial\hat{r}}-\frac{n^2}{\hat{r}^2}+g(\hat{r},p)$$

is not Hermitian. The operator $\mathscr{L}$ with appropriate boundary conditions have three properties that are of importance in our case:

- the eigenvalues of the operator $\mathscr{L}$ are complex;
- the eigenfunctions of the operator $\mathscr{L}$ are orthogonal;
- the eigenfunctions of the operator $\mathscr{L}$ form a complete set.

It is relevant to mention that the orthogonality and the normalization conditions are formulated without complex conjugation:

$$\int_0^\infty \Psi_{nj}(\hat{r})\Psi_{ni}(\hat{r})\hat{r}\,\mathrm{d}\hat{r}=\delta_{ij}.$$

In this spirit, let us introduce inhomogeneous differential equation associated with Eq. (12):

$$\mathscr{L}\Psi_n+\Lambda\Psi_n=f^{(n)}(\hat{r}). \tag{16}$$

This equation can be solved by utilizing a Green's-function technique:

$$\Psi_n=\int_0^\infty G^{(n)}(\hat{r},\hat{r}')f^{(n)}(\hat{r}')\hat{r}'\,\mathrm{d}\hat{r}'.$$

We expand the Green's function in a series of eigenfunctions of the associated homogeneous equation (15), that is

$$G^{(n)}(\hat{r},\hat{r}')=-\sum_j\frac{\Psi_{nj}(\hat{r})\Psi_{nj}(\hat{r}')}{\Lambda-\Lambda_j^{(n)}}.$$

Now we let $\Lambda=2\mathrm{i}Bp$ and write down the corresponding Green's function of the inhomogeneous equation (12) determining $\bar{E}^{(n)}$:

$$G^{(n)}(\hat{r},\hat{r}') = -\sum_j \frac{\Psi_{nj}(\hat{r})\Psi_{nj}(\hat{r}')}{2\mathrm{i}Bp - \Lambda_j^{(n)}}.$$

Finally, $\bar{E}^{(n)}(\hat{r},p)$, the desired solution of Eq. (11), is given by

$$\bar{E}^{(n)}(\hat{r},p) = -\sum_j \frac{\Psi_{nj}(\hat{r})}{2\mathrm{i}Bp - \Lambda_j^{(n)}} \int_0^\infty \Psi_{nj}(\hat{r}')f^{(n)}(\hat{r}')\hat{r}'\,\mathrm{d}\hat{r}',$$

where $\Lambda_j^{(n)}(p)$ is the eigenvalue and $\Psi_{nj}(\hat{r},p)$, the orthonormal eigenfunction of the associated homogeneous differential equation (15).

To find $\hat{E}^{(n)}(\hat{z},\hat{r})$, we use the inverse Laplace transformation:

$$\widetilde{E}^{(n)}(\hat{z},\hat{r}) = \frac{1}{2\pi\mathrm{i}} \int_{\alpha-\mathrm{i}\infty}^{\alpha+\mathrm{i}\infty} \mathrm{d}p\bar{E}^{(n)}(p,\hat{r})\mathrm{e}^{p\hat{z}},$$

where integration path in the complex plane p is parallel to the imaginary axis. The real constant α is larger than the real parts of all the singularities of $\bar{E}^{(n)}(p,\hat{r})$. We shall consider only the high-gain limit. If the undulator is sufficiently long, the contributions of the residues at $p = \lambda_j^{(n)}$ proportional to $\exp(\lambda_j^{(n)}\hat{z})$ with $\mathrm{Re}(\lambda_j^{(n)}) > 0$ are larger than all the other terms, and the contributions of the latter can be neglected. In this case the solution for the field amplitude $\hat{E}^{(n)}(\hat{z},\hat{r})$ takes the form:

$$\widetilde{E}^{(n)}(\hat{z},\hat{r}) = -\sum_j \exp(\lambda_j^{(n)}\hat{z})\Phi_{nj}(\hat{r}) \left[2\mathrm{i}B - \left(\frac{\mathrm{d}\Lambda_j^{(n)}}{\mathrm{d}p}\right)_{p=\lambda_j^{(n)}}\right]^{-1} \int_0^\infty \Phi_{nj}(\hat{r}')f^{(n)}(\hat{r}',\lambda_j^{(n)})\hat{r}'\,\mathrm{d}\hat{r}', \tag{17}$$

where the eigenfunctions $\Phi_{nj}(\hat{r}) = \Psi_{nj}(\hat{r},p = \lambda_j^{(n)})$ are solutions of the Eq. (13).

Let us derive explicit expression for the derivative of eigenvalue with respect to p at the point $p = \lambda_j^{(n)}$. Using associated eigenvalue equation (15) and normalization condition,

$$\int_0^\infty \Psi_{nj}^2(\hat{r})\hat{r}\,\mathrm{d}\hat{r} = 1,$$

we find

$$\Lambda_j^{(n)} = -\int_0^\infty \Psi_{nj}(\hat{r})\left[\frac{\partial^2}{\partial\hat{r}^2} + \frac{1}{\hat{r}}\frac{\partial}{\partial\hat{r}} - \frac{n^2}{\hat{r}^2} + g(\hat{r},p)\right]\Psi_{nj}(\hat{r})\hat{r}\,\mathrm{d}\hat{r}.$$

Note that the eigenfunctions of the operator $\mathscr{L}$ are orthogonal and form a complete set. Thus, we have

$$\frac{\mathrm{d}\Lambda_j^{(n)}}{\mathrm{d}p} = -\int_0^\infty \Psi_{nj}^2(\hat{r})\frac{\partial g(\hat{r},p)}{\partial p}\hat{r}\,\mathrm{d}\hat{r}.$$

For the case of Schrödinger's equation, we explain the last relation by saying that the first-order change in eigenvalue is equal to the "expectation" value of the perturbing potential over the unperturbed states.

2.2.2. Input coupling factors

The analytical results obtained above describe the high-gain linear regime of FEL amplifier. At a sufficient distance from the undulator entrance the output radiation can be presented as a superposition of the "self-reproducing" field configurations:

$$\hat{E}^{(n)}(\hat{z},\hat{r}) = \sum_j A_j^{(n)}\Phi_{nj}(\hat{r})\exp(\lambda_j^{(n)}\hat{z}). \tag{18}$$

The term "self-reproducing" refers to the fact that the transverse dependence of the field is independent of the axial coordinate z. The complex eigenvalues have positive real part, $\mathrm{Re}(\lambda_j^{(n)}) > 0$, since these correspond to exponential growth in z. The input coupling factors $A_j^{(n)}$ are given by the expression

$$A_j^{(n)} = 4\mathrm{i}v_j^{(n)} \int_0^\infty \hat{a}_{\mathrm{ext}}^{(n)}(\hat{r}) S(\hat{r}) \Phi_{nj}(\hat{r}) \hat{r}\, \mathrm{d}\hat{r}.$$

Here we use the following notation

$$v_j^{(n)} = \hat{D}_0(\lambda_j^{(n)}) \left[2\mathrm{i}B + \int_0^\infty \Phi_{nj}^2(\hat{r}) \left(\frac{\mathrm{d}g(\hat{r},p)}{\mathrm{d}p} \right)_{p=\lambda_j^{(n)}} \hat{r}\, \mathrm{d}\hat{r} \right]^{-1}.$$

For simplicity, in this article we confined our attention to the situations where space charge effects are negligible, $\hat{\Lambda}_{\mathrm{p}}^2 \to 0$. However, the reader can simply extend the analysis with this effects taken into account. The field amplitude is then given by Eq. (18). The expression for input coupling factors now reduces to [17,19]:

$$A_j^{(n)} = 2u_j^{(n)} \int_0^\infty \hat{a}_{\mathrm{ext}}^{(n)}(\hat{r}) S(\hat{r}) \Phi_{nj}(\hat{r}) \hat{r}\, \mathrm{d}\hat{r},$$

where $u_j^{(n)}$ can be written in the following form:

$$u_j^{(n)} = \hat{D}_0(\lambda_j^{(n)}) \left[B \int_0^\infty \Phi_{nj}^2(\hat{r}) \hat{r}\, \mathrm{d}\hat{r} - \left(\frac{\mathrm{d}\hat{D}}{\mathrm{d}p} \right)_{p=\lambda_j^{(n)}} \int_0^\infty \Phi_{nj}^2(\hat{r}) S(\hat{r}) \hat{r}\, \mathrm{d}\hat{r} \right]^{-1}.$$

Here and below it is convenient to use eigenfunctions without normalization condition.

2.2.3. Calculation of output power

An important characteristic of the FEL amplifier is the output power. In the paraxial approximation the diffraction angles are small, the vectors of the electric and magnetic field are perpendicular to each other and have equal absolute values. Thus the expression for the power of the radiation with azimuthal index n, can be written in the form:

$$W^{(n)} = \frac{c}{4\pi} \int_0^\infty |\widetilde{E}^{(n)}|^2 2\pi r\, \mathrm{d}r. \tag{19}$$

Introducing the notion of the electron beam power, $W_{\mathrm{b}} = \mathscr{E}_0 I_0/e$, we rewrite Eq. (19) in the following normalized form:

$$\hat{W}^{(n)} = \frac{W^{(n)}}{\rho W_{\mathrm{b}}} = \frac{B}{4} \int_0^\infty |\hat{E}^{(n)}(\hat{z},\hat{r})|^2 \hat{r}\, \mathrm{d}\hat{r} \left[\int_0^\infty \zeta S(\zeta)\, \mathrm{d}\zeta \right]^{-1}. \tag{20}$$

Thus, the exact solution of the initial-value problem for FEL amplifier with arbitrary gradient profile has been derived (as mentioned in Section 1, we applied a method of solution, originally introduced by Krinsky and Yu [19]). As a result, if we have information on the eigenfunctions and eigenvalues, we are able to calculate radiation properties of the FEL amplifier which operates in high-gain linear regime.

2.3. A systematic approach for the determination of eigenmode

The eigenvalue problem for the case of an arbitrary gradient axisymmetric profile is solved by means of the multilayer approximation method (see Refs. [20,21] for more details). Let $\hat{r}_{\mathrm{b}}$ be the normalized radius of

the beam boundary. We divide the region $0 < \hat{r} < \hat{r}_b$ into K layers. The beam current density is assumed to be constant within each layer. According to Eq. (13), the solution for the eigenfunction within each layer is

$$\Phi_n^{(k)} = c_k J_n(\mu_k \hat{r}) + d_k N_n(\mu_k \hat{r}),$$

where $(k-1)/K < \hat{r} < k\hat{r}_b/K$, c_k and d_k are constants, J_n and N_n are the Bessel functions of the first and second kind of order n respectively, and

$$\mu_k^2 = 2i\hat{D}S_{k-1/2} - q^2, \quad q^2 = -2iB\Lambda,$$

where $S_{k-1/2} = S(\hat{r}_{k-1/2})$ and $\hat{r}_{k-1/2} = \hat{r}_b(k-1/2)/K$. To avoid a singularity of the eigenfunction at $\hat{r} = 0$, we should let $d_1 = 0$. All the other coefficients are obtained from the continuity conditions for the eigenfunction and its derivative at the boundaries between the layers. These equations can be written in the matrix form:

$$\begin{pmatrix} c_{k+1} \\ d_{k+1} \end{pmatrix} = T_k \begin{pmatrix} c_k \\ d_k \end{pmatrix}, \quad k = 1, 2, \ldots, K-1, \tag{21}$$

where the coefficients T_k are given by ($\hat{r}_k = \hat{r}_b k/K$):

$$\begin{aligned}
(T_k)_{11} &= (\pi/2)\hat{r}_k[\mu_k J_{n+1}(\mu_k \hat{r}_k) N_n(\mu_{k+1}\hat{r}_k) - \mu_{k+1} J_n(\mu_k \hat{r}_k) N_{n+1}(\mu_{k+1}\hat{r}_k)], \\
(T_k)_{12} &= (\pi/2)\hat{r}_k[\mu_k N_{n+1}(\mu_k \hat{r}_k) N_n(\mu_{k+1}\hat{r}_k) - \mu_{k+1} N_n(\mu_k \hat{r}_k) N_{n+1}(\mu_{k+1}\hat{r}_k)], \\
(T_k)_{21} &= -(\pi/2)\hat{r}_k[\mu_k J_{n+1}(\mu_k \hat{r}_k) J_n(\mu_{k+1}\hat{r}_k) - \mu_{k+1} J_n(\mu_k \hat{r}_k) J_{n+1}(\mu_{k+1}\hat{r}_k)], \\
(T_k)_{22} &= -(\pi/2)\hat{r}_k[\mu_k N_{n+1}(\mu_k \hat{r}_k) J_n(\mu_{k+1}\hat{r}_k) - \mu_{k+1} N_n(\mu_k \hat{r}_k) J_{n+1}(\mu_{k+1}\hat{r}_k)].
\end{aligned} \tag{22}$$

According to Eq. (13), the solution for the eigenfunction outside the beam, $\hat{r} > \hat{r}_b$, satisfying the condition of the quadratic integrability is

$$\Phi_{(n)}(\hat{r}) = bK_n(q\hat{r}), \quad \mathrm{Re}(q) > 0.$$

At the beam boundary, at $\hat{r} = \hat{r}_b$, the continuity condition gives the following relations:

$$c_K J_n(\mu_K \hat{r}_b) + d_K N_n(\mu_K \hat{r}_b) = bK_n(q\hat{r}_b),$$

$$\mu_K c_K J_{n+1}(\mu_K \hat{r}_b) + \mu_K d_K N_{n+1}(\mu_K \hat{r}_b) = qbK_{n+1}(q\hat{r}_b),$$

which can be written in the matrix form

$$T_K \begin{pmatrix} c_K \\ d_K \end{pmatrix} = b \begin{pmatrix} 1 \\ 1 \end{pmatrix}. \tag{23}$$

The coefficient b can be expressed in terms of the coefficient c_1 by multiple use of Eq. (21). The coefficient c_1 may be chosen arbitrary, so without loss of generality we let $c_1 = 1$. Then we can write the following matrix equation:

$$T_K \times T_{K-1} \times \cdots \times T_1 \begin{pmatrix} 1 \\ 0 \end{pmatrix} = T \begin{pmatrix} 1 \\ 0 \end{pmatrix} = b \begin{pmatrix} 1 \\ 1 \end{pmatrix}, \tag{24}$$

where the matrix T depends on the unknown quantity $\hat{\Lambda}$. Another unknown quantity in Eq. (24) is the coefficient b, which can be easily excluded. Thus, we obtain the eigenvalue equation

$$(T)_{11} = (T)_{21}, \tag{25}$$

which allows one to find the eigenvalue $\hat{\Lambda}$. The eigenfunction is calculated using Eqs. (21) and (23).

2.4. Electron beam with Gaussian profile

Now let us consider a beam with Gaussian distribution of the current density:

$$j_0(r) = \frac{I_0}{2\pi\sigma^2}\exp\left(-\frac{r^2}{2\sigma^2}\right).$$

It is reasonable to choose the rms radius, $\sqrt{2}\sigma$, as the profile parameter r_0. The profile function is

$$S(\hat{r}) = \exp(-\hat{r}^2), \tag{26}$$

where $\hat{r} = r/(\sqrt{2}\sigma)$. The reduced parameters in the case of the Gaussian profile are as follows:

$$\Gamma = \left[I_0\omega^2\theta_s^2(I_A c^2\gamma_z^2\gamma)^{-1}\right]^{1/2}, \qquad B = 2\sigma^2\Gamma\omega/c.$$

We substitute Eq. (26) into Eq. (20) and obtain

$$\hat{W}^{(n)} = \frac{B}{2}\int_0^\infty |\hat{E}^{(n)}|\hat{r}\,\mathrm{d}\hat{r}, \tag{27}$$

$$\hat{E}^{(n)}(\hat{z},\hat{r}) = \sum_j A_j^{(n)}\Phi_{nj}(\hat{r})\exp(\lambda_j^{(n)}\hat{z}), \tag{28}$$

where

$$A_j^{(n)} = 2u_j^{(n)}\int_0^\infty \hat{a}_{\mathrm{ext}}^{(n)}(\hat{r})\exp(-\hat{r}^2)\Phi_{nj}(\hat{r})\hat{r}\,\mathrm{d}\hat{r},$$

$$u_j^{(n)} = \hat{D}_0(\lambda_j^{(n)})\left[B\int_0^\infty \Phi_{nj}^2(\hat{r})\hat{r}\,\mathrm{d}\hat{r} - \left(\frac{\mathrm{d}\hat{D}}{\mathrm{d}p}\right)_{p=\lambda_j}\int_0^\infty \Phi_{nj}^2(\hat{r})\exp(-\hat{r}^2)\hat{r}\,\mathrm{d}\hat{r}\right]^{-1}.$$

2.4.1. Gaussian energy spread

For a Gaussian energy spread in the electron beam, the functions $\hat{D}(p)$ and $\hat{D}_0(p)$ are given by

$$\hat{D} = \mathrm{i}\int_0^\infty \xi\exp\left[-\hat{\Lambda}_T^2\xi^2/2 - (p+\mathrm{i}\hat{C})\xi\right]\mathrm{d}\xi,$$

$$\hat{D}_0 = \int_0^\infty \exp\left[-\hat{\Lambda}_T^2\xi^2/2 - (p+\mathrm{i}\hat{C})\xi\right]\mathrm{d}\xi.$$

Taking into account the definition of the function $\hat{D}(\lambda)$, we get

$$\left(\frac{\mathrm{d}\hat{D}}{\mathrm{d}p}\right)_{p=\lambda_j^{(n)}} = \left(\hat{D}(\lambda_j^{(n)}) - \frac{\mathrm{i}}{\hat{\Lambda}_T^2}\right)\left(\frac{1}{\lambda_j^{(n)}+\mathrm{i}\hat{C}} + \frac{\lambda_j^{(n)}+\mathrm{i}\hat{C}}{\hat{\Lambda}_T^2}\right) + \frac{\mathrm{i}\left(\lambda_j^{(n)}+\mathrm{i}\hat{C}\right)}{\hat{\Lambda}_T^4}.$$

In the limit of negligibly small energy spread, $\hat{\Lambda}_T^2 \to 0$, the function $\hat{D}$ and its derivative with respect to λ at $\lambda = \lambda_j^{(n)}$ takes the following simple form:

$$\hat{D}(\lambda_j^{(n)}) = \frac{\mathrm{i}}{(\lambda_j^{(n)}+\mathrm{i}\hat{C})^2}, \quad \left(\frac{\mathrm{d}\hat{D}}{\mathrm{d}p}\right)_{p=\lambda_j^{(n)}} = -\frac{2\mathrm{i}}{(\lambda_j^{(n)}+\mathrm{i}\hat{C})^3}.$$

3. Start-up from shot noise

Fluctuations of the electron beam current density serve as the input signal in the SASE FEL. These fluctuations always exist in the electron beam due to the effect of shot noise. Let us consider the microscopic picture of the electron beam current density at the entrance to the undulator. The shot noise in the electron beam causes fluctuations of the beam current density which are random in time and space. As a result, the beam current density at the entrance to the undulator can be written in the form:

$$j_z(\vec{r}_\perp,t,z)\big|_{z=0} = (-e)\sum_{k=1}^{N}\delta(t-t_k)\delta(\vec{r}_\perp-\vec{r}_\perp^{(k)}),$$

where $\delta(\cdot)$ is the delta function, $(-e)$ is the charge of the electron, N is the number of the electrons in a bunch, t_k and $\vec{r}_\perp^{(k)}$ are the random arrival time and transverse coordinate of the kth electron at the undulator entrance. The beam current density averaged over an ensemble of bunches can be written in the form:

$$\langle j_z(\vec{r}_\perp,0,t)\rangle = -j_0(\vec{r}_\perp)F(t),$$

where $F(t)$ is the longitudinal profile function. The averaging symbol $\langle\cdot\rangle$ means the ensemble average over bunches. In this paper we shall consider a rectangular electron bunch of sufficient duration, T, such as $\rho\omega_0 T \gg 1$, where ω_0 is the resonance frequency and ρ is the efficiency parameter. The physical interpretation of this approximation is that the electron bunch is much longer than the slippage of the radiation with respect to the electrons per gain length. It allows us to neglect edge effects and to use the steady-state Green's function for any frequency within the FEL bandwidth. It is assumed that only the fluctuations of the beam current density define the value of input signal. This means that we can neglect the effect of longitudinal velocity fluctuations connected with the finite energy spread in the beam.

3.1. Average radiation power

We start with the calculation of the average radiation power at the undulator exit. The components of electric field of the electromagnetic wave in the time domain, $E_{x,y}(\vec{r}_\perp,t)$ and its Fourier transform, $\bar{E}_{x,y}(\vec{r}_\perp,\omega)$, are connected by

$$E_{x,y}(\vec{r}_\perp,z,t) = \frac{1}{2\pi}\int_{-\infty}^{\infty}\bar{E}_{x,y}(\vec{r}_\perp,z,\omega)\mathrm{e}^{-\mathrm{i}\omega t}\mathrm{d}\omega.$$

Using the expression for Poynting's vector and Parseval's theorem, we calculate the radiation energy in one radiation pulse:

$$\begin{aligned}\mathscr{E} &= \frac{c}{4\pi}\int \mathrm{d}\vec{r}_\perp\int_0^T \mathrm{d}t\left[E_x^2(\vec{r}_\perp,z,t)+E_y^2(\vec{r}_\perp,z,t)\right]\\ &= \frac{c}{4\pi^2}\int \mathrm{d}\vec{r}_\perp\int_0^\infty \mathrm{d}\omega\left[|\bar{E}_x(\vec{r}_\perp,z,\omega)|^2+|\bar{E}_y(\vec{r}_\perp,z,\omega)|^2\right].\end{aligned} \tag{29}$$

Taking into account that radiation field is circularly polarized, i.e. $\bar{E}_x = \mathrm{i}\bar{E}_y$, we obtain that

$$\mathscr{E} = \frac{c}{8\pi^2}\int \mathrm{d}\vec{r}_\perp\int_0^\infty \mathrm{d}\omega|\bar{E}_x(\vec{r}_\perp,z,\omega)+\mathrm{i}\bar{E}_y(\vec{r}_\perp,z,\omega)|^2. \tag{30}$$

Let us recall some results of the steady-state 3-D theory of the FEL amplifier. In Section 2 we considered the special case of initial conditions when the electron beam, modulated in frequency ω, is fed to the undulator entrance. The output radiation also has the same frequency, ω. In the high-gain linear regime the radiation can be presented as a superposition of the exponentially growing guiding modes. In this section we study the case when the initial modulation of the electron beam is defined by the shot noise and has a white spectrum. Under the accepted limitations the results of the steady-state theory can be extended to this complicated case. Indeed, we can decompose the input signal into Fourier harmonics:

$$\bar{j}_{\mathrm{ext}}(\vec{r}_\perp,\omega)=\int_{-\infty}^{\infty}\mathrm{d}t\,\mathrm{e}^{\mathrm{i}\omega t}j_z(\vec{r}_\perp,z,t)|_{z=0}=(-e)\sum_{k=1}^{N}\mathrm{e}^{\mathrm{i}\omega t_k}\delta(\vec{r}_\perp-\vec{r}_\perp^{(k)}).$$

Since in the linear regime all the harmonics are amplified independently, we can use the result of steady-state theory (28) for each harmonic and calculate the corresponding Fourier harmonics of output radiation field. For $\omega>0$ the asymptotic expression for the harmonic of the field takes the form:

$$\bar{E}_x^{(n)}(r,z,\omega)+\mathrm{i}\bar{E}_y^{(n)}(r,z,\omega)=\sum_j 2\mathrm{e}^{\mathrm{i}\omega z/c}u_j^{(n)}\Phi_{nj}(\hat{r})\exp(\lambda_j^{(n)}\hat{z})\left[\sum_{k=1}^{N}\Phi_{nj}(\hat{r}^{(k)})\exp(-\mathrm{i}n\varphi_k+\mathrm{i}\omega t_k)\right]\times\left(2\pi\int_0^{\infty}S(\hat{r})\hat{r}\,\mathrm{d}\hat{r}\right)\frac{E_0}{I_0}. \tag{31}$$

When $\omega<0$ the Fourier harmonics defined by the relation $\bar{E}_{x,y}^{(n)}(r,z,-\omega)=(\bar{E}_{x,y}^{(n)}(r,z,\omega))^*$. It should be noted that eigenvalues $\lambda_j^{(n)}$, eigenfunctions Φ_{nj} and coefficients $u_j^{(n)}$ are universal functions of the detuning parameter $\hat{C}=(\omega_0-\omega)/(2\rho\omega_0)$. Substituting expression (31) in Eq. (29) we obtain the radiation energy in one pulse. Then we divide the result by the pulse duration, T, and average over an ensemble. This gives us the averaged radiation power

$$\langle\hat{W}\rangle=\langle W\rangle/(\rho W_{\mathrm{b}})=\sum_n\langle\hat{W}^{(n)}\rangle, \tag{32}$$

where the contribution of the radiation with azimuthal index n to the total radiation power is given by the expression [17,19]:

$$\langle\hat{W}^{(n)}\rangle=\frac{B}{\pi N_{\mathrm{c}}}\int_{-\infty}^{\infty}\mathrm{d}\hat{C}\left\{\sum_{k,j}u_k^{(n)}(u_j^{(n)})^*\exp\left\{[\lambda_k^{(n)}+(\lambda_j^{(n)})^*]\hat{z}\right\}\times\int_0^{\infty}\Phi_{nk}(\hat{r})\Phi_{nj}^*(\hat{r})S(\hat{r})\hat{r}\,\mathrm{d}\hat{r}\int_0^{\infty}\Phi_{nk}(\hat{r})\Phi_{nj}^*(\hat{r})\hat{r}\,\mathrm{d}\hat{r}\right\}, \tag{33}$$

where $N_{\mathrm{c}}=N_\lambda/(2\pi\rho)$, $N_\lambda=2\pi I_0/(e\omega_0)$ is the number of electrons per radiation wavelength, $I_0=eN/T$ is the average beam current. The parameters of the SASE FEL are usually chosen in such a way that transverse coherence is achieved at the end of amplification process. This happens due to transverse mode selection, i.e. only one ground mode survives in the end. For this limit we can write the following asymptotic expression for the output power:

$$\langle\hat{W}\rangle=\frac{B}{\pi N_{\mathrm{c}}}\int_{-\infty}^{\infty}\mathrm{d}\hat{C}\left\{\exp[2\mathrm{Re}(\lambda_0^{(0)})\hat{z}]|\hat{D}_0|^2\left|B\int_0^{\infty}\Phi_{00}^2(\hat{r})\hat{r}\,\mathrm{d}\hat{r}-\left(\frac{\mathrm{d}\hat{D}}{\mathrm{d}p}\right)_{p=\lambda_0^{(0)}}\int_0^{\infty}\Phi_{00}^2(\hat{r})S(\hat{r})\hat{r}\,\mathrm{d}\hat{r}\right|^{-2}\times\int_0^{\infty}|\Phi_{00}(\hat{r})|^2S(\hat{r})\hat{r}\,\mathrm{d}\hat{r}\int_0^{\infty}|\Phi_{00}(\hat{r})|^2\hat{r}\,\mathrm{d}\hat{r}\right\}. \tag{34}$$

3.2. Averaged angular distribution of the radiation intensity

At a sufficiently large undulator length the spectrum of the SASE radiation is concentrated within the narrow band near the resonance frequency ω_0. Therefore, the electric field of the wave can be presented as

$$E_x + \mathrm{i}E_y = \widetilde{E}(\vec{r}_\perp, z, t)\mathrm{e}^{\mathrm{i}\omega_0(z/c-t)} + \text{c.c.},$$

where $\widetilde{E}$ is the slowly varying complex amplitude. The next problem of interest is the angular distribution of the radiation intensity. The radiation field at the undulator exit may be written as a superposition of plane waves. The spatial Fourier transform of the complex amplitude $\widetilde{E}$ is

$$A(\vec{k}_\perp, z, t) = \int \widetilde{E}(\vec{r}_\perp, z, t)\exp(-\mathrm{i}\vec{k}_\perp\vec{r}_\perp)\,\mathrm{d}\vec{r}_\perp. \tag{35}$$

Then the averaged angular spectrum can be written as

$$h(\vec{k}_\perp, z) = \frac{\langle|A(\vec{k}_\perp, z, t)|^2\rangle}{\int\langle|A(\vec{k}_\perp, z, t)|^2\,\mathrm{d}\vec{k}_\perp}.$$

Taking into account Eq. (35) and Parseval's theorem, we obtain

$$h(\vec{k}_\perp, z) = \frac{\int\int\langle\widetilde{E}(\vec{r}_\perp, z, t)\widetilde{E}^*(\vec{r}'_\perp, z, t)\rangle\exp[-\mathrm{i}\vec{k}_\perp(\vec{r}_\perp - \vec{r}'_\perp)]\,\mathrm{d}\vec{r}_\perp\,\mathrm{d}\vec{r}'_\perp}{(2\pi)^2\int\langle|\widetilde{E}(\vec{r}_\perp, z, t)|^2\rangle\,\mathrm{d}\vec{r}_\perp}.$$

Using the notation $\vec{\rho} = \vec{r}_\perp - \vec{r}'_\perp$ and $\vec{R} = (\vec{r}_\perp + \vec{r}'_\perp)/2$, we can rewrite the latter expression as

$$h(\vec{k}_\perp, z) = \frac{\int\int\langle\widetilde{E}(\vec{R} + \vec{\rho}/2, z, t)\widetilde{E}^*(\vec{R} - \vec{\rho}/2, z, t)\rangle\exp(-\mathrm{i}\vec{k}_\perp\vec{\rho})\,\mathrm{d}\vec{\rho}\,\mathrm{d}\vec{R}}{(2\pi)^2\int\langle|\widetilde{E}(\vec{R}, z, t)|^2\rangle\,\mathrm{d}\vec{R}}.$$

Then we can introduce the definition of effective transverse correlation function:

$$\gamma^{\mathrm{eff}}(\vec{\rho}, z) = \frac{\int\langle\widetilde{E}(\vec{R} + \vec{\rho}/2, z, t)\widetilde{E}^*(\vec{R} - \vec{\rho}/2, z, t)\rangle\,\mathrm{d}\vec{R}}{\int\langle|\widetilde{E}(\vec{R}, z, t)|^2\rangle\,\mathrm{d}\vec{R}}.$$

The angular spectrum and the effective correlation function are connected by the Fourier transform

$$h(\vec{k}_\perp, z) = \frac{1}{(2\pi)^2}\int\gamma^{\mathrm{eff}}(\vec{\rho}, z)\exp(-\mathrm{i}\vec{k}_\perp\vec{\rho})\,\mathrm{d}\vec{\rho}.$$

Thus, the averaged intensity distribution in the far zone $h(\vec{k}_\perp, z)$ is totally defined by the effective transverse correlation function. On the other hand, if one knows $h(\vec{k}_\perp, z)$, then $\gamma^{\mathrm{eff}}(\vec{\rho}, z)$ can be calculated by means of the inverse Fourier transformation.

Let us consider a axisymmetric electron beam. Using cylindrical coordinates we represent output power as a Fourier series in the azimuthal angle φ:

$$\widetilde{E}(z, r, \varphi, t) = \sum_{n=-\infty}^{n=+\infty}\widetilde{E}^{(n)}(z, r, t)\mathrm{e}^{-\mathrm{i}n\varphi}.$$

The radiation field at the undulator exit may be written as a superposition of plane waves. The value $k_\perp/k$ gives the sine of the angle between the z axis and the direction of propagation of the plane wave with the wave number $k = \omega/c$. In paraxial approximation $k_\perp/k = \sin(\theta) \simeq \theta$. The spatial Fourier transform of the radiation field is given by

$$A(\theta,\varphi,z,t)=\sum_n \mathrm{e}^{-\mathrm{i}n\varphi}\Xi^{(n)}(\theta,z,t)=2\pi\sum_n \mathrm{e}^{-\mathrm{i}n(\varphi+\pi/2)}\int_0^\infty \hat{E}^{(n)}(r,z,t)J_n(\theta\omega_0 r/c)r\,\mathrm{d}r, \tag{36}$$

where J_n is the Bessel function of first kind. In the case of axisymmetric electron beam statistical process is isotropic. Then the averaged angular spectrum can be written as

$$h(\theta,z)=\left[\sum_n\langle|\Xi^{(n)}(\theta,z,t)|^2\rangle\right]\left[2\pi\frac{\omega_0^2}{c^2}\sum_n\int\langle|\Xi^{(n)}(\theta,z,t)|^2\rangle\theta\,\mathrm{d}\theta\right]^{-1}.$$

Using Eq. (36) and Parseval's theorem we obtain

$$\begin{aligned}h(\theta,z)=&\left[\sum_n\int_0^\infty\int_0^\infty\langle\hat{E}^{(n)}(r,z,t)(\widetilde{E}^{(n)}(r',z,t))^*\rangle J_n(\theta\omega_0 r/c)J_n(\theta\omega_0 r'/c)rr'\,\mathrm{d}r\,\mathrm{d}r'\right]\\&\times\left[2\pi\sum_n\int_0^\infty\langle|\widetilde{E}_{(n)}(r,z,t)|^2\rangle r\,\mathrm{d}r\right]^{-1}.\end{aligned} \tag{37}$$

Since in the linear regime all the harmonics are amplified independently, we can use in high-gain regime the asymptotic result of steady-state theory (31) for each Fourier harmonics of output radiation. Finally, the angular spectrum is written in the following dimensionless form:

$$\begin{aligned}h(\hat{\theta},\hat{z})=&\left[\sum_{n,k,j}\int_{-\infty}^\infty\mathrm{d}\hat{C}\left(\Omega_{kj}^{(n)}\int_0^\infty\Phi_{nk}(\hat{r})J_n(\hat{\theta}\hat{r})\hat{r}\,\mathrm{d}\hat{r}\int_0^\infty\Phi_{nj}^*(\hat{r}')J_n(\hat{\theta}\hat{r}')\hat{r}'\,\mathrm{d}\hat{r}'\right)\right]\\&\times\left[2\pi\sum_{n,k,j}\int_{-\infty}^\infty\mathrm{d}\hat{C}\left(\Omega_{kj}^{(n)}\int_0^\infty\Phi_{nk}(\hat{r})\Phi_{nj}^*(\hat{r})\hat{r}\,\mathrm{d}\hat{r}\right)\right]^{-1}.\end{aligned} \tag{38}$$

To simplify this expression, we use the following notations: $\hat{\theta}=\theta\omega_0 r_0/c$,

$$\Omega_{kj}^{(n)}=u_k^{(n)}(u_j^{(n)})^*\exp\left\{\left[\lambda_k^{(n)}+\left(\lambda_j^{(n)}\right)^*\right]\hat{z}\right\}\int_0^\infty\Phi_{nk}(\hat{r})\Phi_{nj}^*(\hat{r})S(\hat{r})\hat{r}\,\mathrm{d}\hat{r}.$$

4. An approach for constructing time-dependent numerical simulation codes

Complete calculation of the parameters of the FEL amplifier can be performed only with numerical simulation codes. Time-dependent simulations of the FEL amplifier are being performed by simultaneous solutions of Maxwell's equations and the equations of motion of the electrons. To be specific, in this section we describe a 3-D, time-dependent code FAST developed for simulations of the SASE FEL [3].

The radiation field and the beam current density are presented in the form:

$$E_x+\mathrm{i}E_y=\widetilde{E}(\vec{r}_\perp,z,t)\mathrm{e}^{\mathrm{i}\omega_0(z/c-t)}+\text{c.c.},$$

$$j_z=-j_0(\vec{r}_\perp,z,t)+\tilde{j}_1(\vec{r}_\perp,z,t)\mathrm{e}^{\mathrm{i}\psi}+\text{c.c.},$$

where $\psi=k_\mathrm{w}z+\omega_0(z/c-t)$, and $-j_0$ is the ensemble averaged current density.

We solve the electrodynamic problem using the paraxial approximation. In this case the wave equation may be written in the following form:

$$\left[\vec{\nabla}_\perp + 2\mathrm{i}\frac{\omega_0}{c}\left(\frac{\partial}{\partial z}+\frac{1}{c}\frac{\partial}{\partial t}\right)\right]\widetilde{E}(\vec{r}_\perp,z,t) = -\frac{4\pi\mathrm{i}\theta_\mathrm{s}\omega_0}{c^2}\tilde{j}_1(\vec{r}_\perp,z,t). \tag{39}$$

The solution of this equation is

$$\widetilde{E}(\vec{r}_\perp,z,t) = \frac{\mathrm{i}\theta_\mathrm{s}\omega_0}{c^2}\int_0^z \frac{\mathrm{d}z'}{z-z'}\int \mathrm{d}\vec{r}'_\perp \tilde{j}_1\left(\vec{r}'_\perp,z',t-\frac{z-z'}{c}\right)\exp\left[\frac{\mathrm{i}\omega_0|\vec{r}_\perp-\vec{r}'_\perp|^2}{2c(z-z')}\right]. \tag{40}$$

The complex amplitudes, $\widetilde{E}$ and $\tilde{j}_1$, are expanded in a Fourier series in the angle φ,

$$\widetilde{E} = \sum_{n=-\infty}^{\infty}\widetilde{E}^{(n)}(r,z,t)\mathrm{e}^{-\mathrm{i}n\varphi}, \qquad \tilde{j}_1 = \sum_{n=-\infty}^{\infty}\tilde{j}_1^{(n)}(r,z,t)\mathrm{e}^{-\mathrm{i}n\varphi}.$$

Then we get from Eq. (40) the expression for the Fourier harmonics:

$$\widetilde{E}^{(n)}(r,z,t) = \frac{2\pi\theta_\mathrm{s}\omega_0}{c^2}\mathrm{e}^{-\mathrm{i}n\pi/2}\int_0^z\frac{\mathrm{d}z'}{z-z'}\int_0^\infty \mathrm{d}r'\,r'\tilde{j}_1^{(n)}\left(r',z',t-\frac{z-z'}{c}\right)J_n\left(\frac{\omega_0 rr'}{c(z-z')}\right)\exp\left[\frac{\mathrm{i}\omega_0(r^2+r'^2)}{2c(z-z')}\right]. \tag{41}$$

Prior to the detailed analysis of start-up from noise (i.e. the self-consistent solution of Eq. (39) and the equations of particle motion under the shot noise initial conditions at the undulator entrance), it is relevant to discuss the region of applicability of the paraxial wave equation (39). The paraxial approximation assumes complex amplitude $\widetilde{E}(\vec{r}_\perp,z,t)$ to be a slowly varying function on the scale of the radiation wavelength. When we consider start-up from noise, the beam current, $\tilde{j}_1(\vec{r}_\perp,z,t)$, is not a slowly varying function. The first limitation on the problem parameters means that the undulator should be sufficiently long, $k_\mathrm{w}z \gg 1$. When the latter condition is fulfilled, we still cannot expect correct results in the 3-D case. Indeed, the incoherent undulator radiation has a wide continuous spectrum. When $k_\mathrm{w}z \gg 1$, Eq. (39) correctly describes the fields in the narrow frequency band near the resonance frequency only, $\Delta\omega/\omega_0 \ll 1$. In terms of the far field zone, it gives correct results only for that part of the incoherent undulator radiation which is concentrated within the angle $\Delta\theta \ll 1/\gamma_z$ near the z axis.

When the FEL amplifier starts from the shot noise, a lot of transverse radiation modes are excited at the beginning of the amplification process; the radiation spectrum and the angular distribution in the far zone are relatively large. During the amplification process, the number of transverse radiation modes decreases, and the contribution of the coherent radiation into the total radiation power is increased. Also, the angular distribution of the radiation intensity in the far zone decreases. When it becomes much less than $1/\gamma_z$, we obtain a correct quantitative description of the amplification process starting from the shot noise.

One more relation, connecting the field and the current density, should come from the solution of the dynamical problem. When the space charge field can be neglected, the equations of motion may be written in the form:

$$\frac{\mathrm{d}P}{\mathrm{d}z} = -\frac{\mathrm{i}e\theta_\mathrm{s}}{2}\widetilde{E}\mathrm{e}^{\mathrm{i}\psi} + \mathrm{c.c.},$$

$$\frac{\mathrm{d}\psi}{\mathrm{d}z} = \omega P/(c\gamma_z^2\mathscr{E}_0).$$

To perform the simulations, we divide the electron beam into a large number of elementary volumes. The size of the divisions of the electron beam in the longitudinal direction should typically be chosen equal to the radiation wavelength. The number of azimuthal harmonics for calculations of the radiation field, N_φ, defines the number of azimuthal divisions of the electron beam. Typically, it should be by an order of magnitude larger than N_φ. Finally, the radial mesh should be chosen. The simulations are performed with a

macroparticle method. The number of macroparticles in each volume is equal to N_m. At each integration step we calculate the bunching, $\hat{a}_1$, in each elementary volume:

$$\hat{a}_1 = \frac{1}{N_m} \sum_{m=1}^{N_m} e^{-i\psi_m}.$$

These values are used to calculate the azimuthal harmonics. The radiation field of the nth azimuthal harmonic in the discrete representation is calculated using the rigorous solution (41). At the next integration step, the sum of the azimuthal harmonics of the field is substituted into the equations of macroparticles motion in each volume, etc. As a result, one can trace the evolution of the radiation field and the particle distribution when the electron beam passes the undulator.

The initial shot noise in the electron beam is simulated according to the algorithm described in Ref. [14]. Since the actual number of particles per elementary volume, N_v, is large, the bunching in each box is the sum of a large number of random phasors with fixed amplitudes and uniformly distributed on $(0, 2\pi)$ phases. Using the central limit theorem, we can conclude that the phases of the bunching parameters are also distributed uniformly and the squared modulus of the amplitudes, $|\hat{a}_1|^2$, are distributed by the negative exponential distribution:

$$p(|\hat{a}_1|^2) = \frac{1}{\langle |\hat{a}_1|^2 \rangle} \exp\left(- \frac{|\hat{a}_1|^2}{\langle |\hat{a}_1|^2 \rangle} \right), \tag{42}$$

where $\langle |\hat{a}_1|^2 \rangle = 1/N_v$. So, a negative exponential random generator with a mean value of $1/N_v$ is used to extract the values of $|\hat{a}_1|^2$ for each volume. The phases of $\hat{a}_1$ are produced by a random number generator for the uniform distribution from 0 to 2π. These values are directly used as input parameters for the linear simulation code. In the nonlinear simulation code the macroparticles are distributed in such a way that the resulting bunching corresponds to the target value of $\hat{a}_1$ in each elementary volume.

The output of the code are the arrays for the field values in the Fresnel diffraction zone. Typical slice for the radiation pulse is presented in Fig. 1. Fig. 2 presents typical temporal structure of the radiation pulse from the FEL amplifier starting from shot noise. Post-processor programs are used to extract additional information for the field distribution in the far diffraction zone, for the spectrum, for the time, space and spectral correlation functions, and for the probability distributions of the radiation power and the radiation energy.

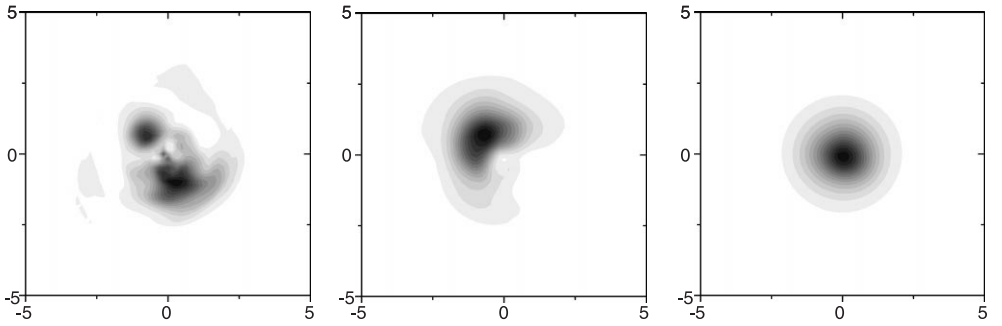


Fig. 1. Distributions of the radiation intensity across one slice of the radiation pulse at different undulator lengths, $\hat{z} = 5$, $\hat{z} = 10$, and $\hat{z} = 15$ (left, middle, and right plots, respectively). The coordinates are normalized to $2^{1/2}\sigma_r$. Here $B = 1$, $\hat{\Lambda}_p^2 \to 0$, and $\hat{\Lambda}_T^2 = 0$. Calculations have been performed with linear simulation code.

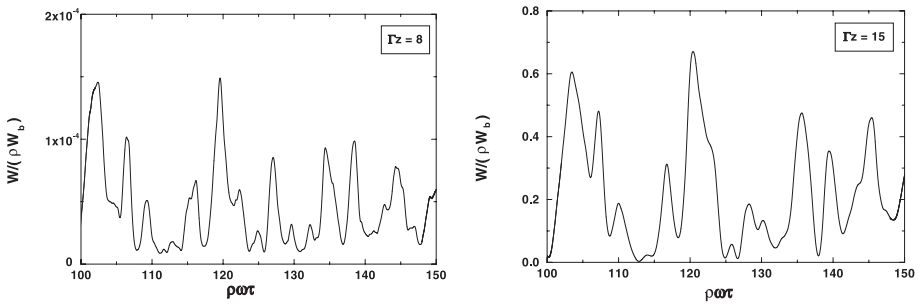


Fig. 2. Temporal structure of the radiation pulse from the FEL amplifier starting from shot noise at the length of undulator of $\hat{z} = 8$ (left plot) and $\hat{z} = 15$ (right plot). Here $B = 1$, $\Lambda_{\mathrm{p}}^2 \to 0$, $\Lambda_T^2 = 0$, and $\hat{z} = 15$. Calculations have been performed with linear simulation code FAST.

5. Comparison of analytical and simulation results

One can easily obtain that identical physical approximations have been used for analytical description of the high-gain linear regime and for numerical simulation algorithm. So, we should expect full agreement of the results in the high-gain linear regime. In other words, analytical results should serve as a primary standard for testing numerical simulation code. To be specific, we present the results for the following set of parameters: diffraction parameter $B = 1$, space charge parameter $\Lambda_{\mathrm{p}}^2 \to 0$, energy spread parameter $\Lambda_T^2 = 0$, and $N_{\mathrm{c}} = 7 \times 10^7$.

Analytical calculations have been performed taking into account nine beam radiation modes, TEM_{mn}, for $m, n = 0, 1, 2$. Numerical simulations have been performed with expansion of the radiation field up to the sixth azimuthal harmonic.

5.1. Averaged radiation power

Fig. 3 shows the evolution of the total radiation power from SASE FEL versus the undulator length. Simulation results have been obtained by means of averaging of the radiation power along the bunch (see Fig. 2). It is seen that analytical and simulation results agree well at $\hat{z} \gtrsim 7$.

Another interesting topic is partial contribution of different beam radiation modes into the total radiation power (see Fig. 4). It is seen that both numerical and analytical results agree well at an increase of the undulator length. One can obtain that numerical simulations always give the value of the radiation power higher than analytical results. The reason is that the numerical simulation code calculates total gain, while the analytical formulae describe only the high-gain asymptote.

5.2. Averaged distributions of the radiation intensity in the near and far zone

Numerical simulation code produces an array containing values for the radiation field in the near zone (see Fig. 1). Averaging of these data over large number of slices gives us averaged distribution of the radiation intensity in the near zone. Relevant analytical quantity is given by expression (33). It is seen from Fig. 5 that there is good agreement between simulation and analytical results.

Analytical predictions for the averaged angular distribution of the radiation power are given by Eq. (38). Similar characteristic can be also calculated with numerical simulation code. Using the values for the radiation field in the near zone, we find the radiation field propagating at any angle in the far diffraction zone. It is seen from Fig. 6 that both approaches agree well in the high-gain linear regime. It is important to stress

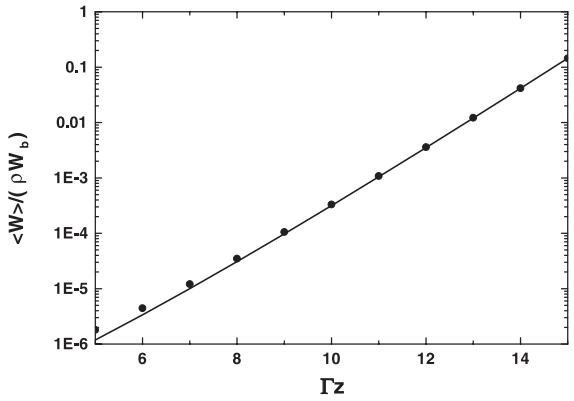


Fig. 3. Averaged power versus undulator length for the FEL amplifier starting from shot noise. Here $B = 1$, $\Lambda_{\mathrm{p}}^2 \to 0$, $\Lambda_T^2 = 0$, and $N_{\mathrm{c}} = 7 \times 10^7$. Solid curve represents analytical results calculated with Eqs. (32) and (33) for nine beam radiation modes ($m, n = 0, 1, 2$). The circles are the results obtained with linear simulation code FAST.

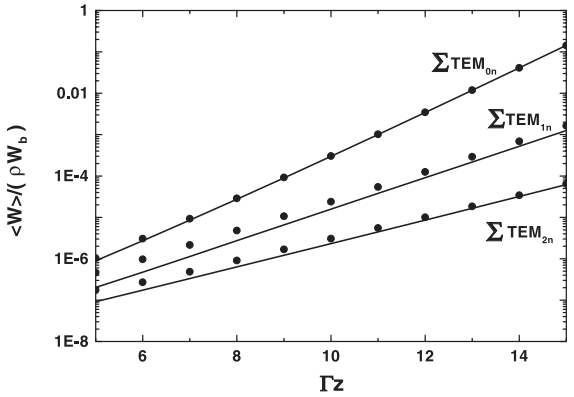


Fig. 4. Partial contributions to the total power (see Fig. 3) of three azimuthal modes with $m = 0$, 1, and 2. Here $B = 1$, $\Lambda_{\mathrm{p}}^2 \to 0$, $\Lambda_T^2 = 0$, and $N_{\mathrm{c}} = 7 \times 10^7$. Solid curves represent analytical results calculated with Eqs. (32) and (33) for sum of three radial modes ($n = 0, 1, 2$). The circles are the results obtained with linear simulation code FAST.

that even after finishing the transverse mode selection process (which takes place after $\hat{z} \gtrsim 10$ for the considered numerical example) the distribution in the far zone differs visibly from the angular distribution of the fundamental TEM_{00} mode for maximum growth rate calculated in the framework of the steady-state theory (dotted line in Fig. 6).

5.3. Averaged radiation spectrum

As we mentioned above, numerical simulation code produces an array containing values for the radiation field in the near zone. Integral spectrum of the radiation pulse can be calculated in the following way. Using the values for the radiation field in the near zone, we find the radiation field propagating at any angle in the far diffraction zone. At the next step of calculations we find the spectral distribution of the radiation power for each angle, and after integrating over all angles we obtain integral spectrum of the radiation pulse. Typical spectrum of the radiation pulse obtained from numerical simulations is present in Fig. 7.

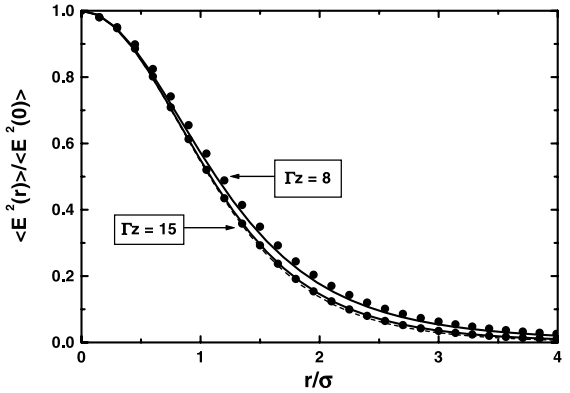


Fig. 5. Averaged distributions of the radiation intensity in the near zone. Here $B = 1$, $\Lambda_p^2 \to 0$, $\Lambda_T^2 = 0$, and $N_c = 7 \times 10^7$. Solid curves represent analytical results calculated with Eq. (33) for sum of three radial modes ($n = 0, 1, 2$). The circles are the results obtained with linear simulation code FAST. Dashed line represents intensity distribution of the fundamental TEM_{00} mode for maximum growth rate calculated in the framework of the steady-state theory.

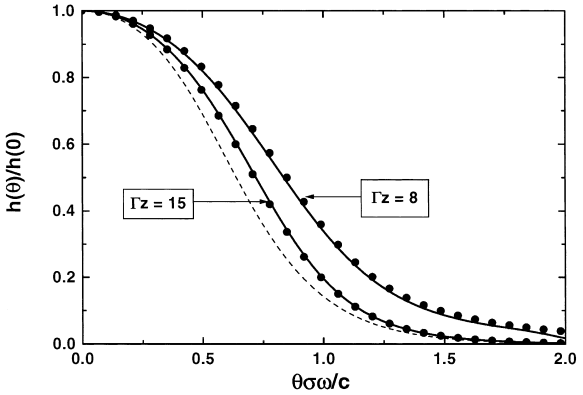


Fig. 6. Averaged angular distribution of the radiation intensity in the far zone for the FEL amplifier starting from shot noise. Here $B = 1$, $\Lambda_p^2 \to 0$, and $\Lambda_T^2 = 0$. Solid curves are the results of analytical calculations with Eq. (38), and the circles are the results obtained with linear simulation code FAST. Dashed line represents angular distribution of the fundamental TEM_{00} mode for maximum growth rate calculated in the framework of the steady-state theory.

Analytical results give predictions for the averaged radiation spectrum (see Eqs. (32) and (33)). To obtain averaged spectrum from numerical simulation code, we performed large number of statistically independent simulation runs. Each run gives spectrum with spiky structure as shown in Fig. 7. Average of a large number of radiation spectra is presented in Fig. 8. It is seen that the analytical and simulation results for the averaged radiation spectrum agree well in the high-gain linear regime.

6. Transverse coherence

In the case of axisymmetric electron beam the radiation field is statistically isotropic. For such a field the effective correlation function depends only on the modulus $|\vec{\rho}|$ and the angular spectrum depends on the modulus $|\vec{k}_\perp|$. Thus, we have

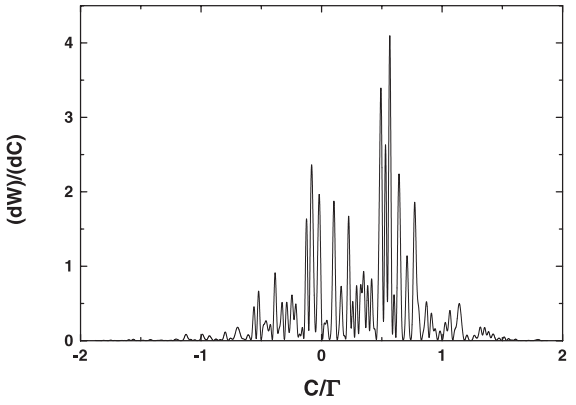


Fig. 7. Typical spectrum of the radiation from the FEL amplifier starting from shot noise at the undulator length $\hat{z} = 15$. Here $B = 1$, $\Lambda_{\mathrm{p}}^2 \to 0$, $\Lambda_T^2 = 0$, and $N_{\mathrm{c}} = 7 \times 10^7$. Calculations have been performed with linear simulation code FAST.

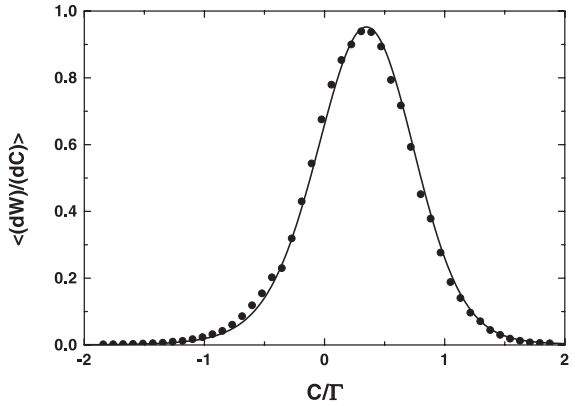


Fig. 8. Averaged spectrum of the radiation from the FEL amplifier starting from shot noise at the undulator length $\hat{z} = 15$. Here $B = 1$, $\Lambda_{\mathrm{p}}^2 \to 0$, $\Lambda_T^2 = 0$, and $N_{\mathrm{c}} = 7 \times 10^7$. Solid curve represents analytical results calculated with Eqs. (32) and (33) for nine beam radiation modes $(m, n = 0, 1, 2)$. The circles are the results obtained with linear simulation code FAST.

$$\gamma_1^{\mathrm{eff}}(\hat{\rho}, \hat{z}) = 2\pi \int_0^{\infty} J_0(\hat{\rho}\hat{\theta}) h(\hat{\theta}) \hat{\theta}\, \mathrm{d}\hat{\theta}, \tag{43}$$

where $\hat{\rho} = |\vec{\rho}|/r_0$. It is natural to define the area of coherence for an isotropic inhomogeneous field as:

$$S_{\mathrm{coh}}(\hat{z}) = 2\pi \int_0^{\infty} |\gamma_1^{\mathrm{eff}}(\hat{\rho}, \hat{z})|^2 \hat{\rho}\, \mathrm{d}\hat{\rho}. \tag{44}$$

Using the relation $S_{\mathrm{coh}} = \pi \hat{r}_{\mathrm{coh}}^2$, it is conventional to introduce the notion of the radius of coherence $\hat{r}_{\mathrm{coh}}$.

To describe the formation of the transverse coherence, we should define the degree of coherence. One possible definition can be made as follows. After statistical analysis of the numerical results we find $\hat{r}_{\mathrm{coh}}$. Then we find the radius of coherence $\hat{r}_{\max}$ for the fully coherent radiation which is represented by the fundamental $\Phi_{00}(\hat{r})$ mode for maximum growth rate. The field distribution of this mode for Gaussian density distribution in the electron beam can be found by the multilayer approximation method described in Section 2.2. The degree of coherence, ζ, may be defined as

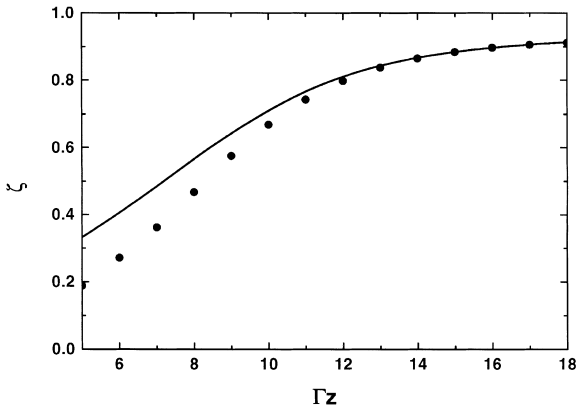


Fig. 9. Degree of transverse coherence of the radiation from the FEL amplifier versus the undulator length. Solid curve represents analytical results, and the circles are the results obtained with linear simulation code FAST. Here $B = 1$, $\Lambda_{\rm p}^2 \to 0$, $\Lambda_T^2 = 0$, and $N_{\rm c} = 7 \times 10^7$.

$$\zeta = \hat{r}_{\rm coh}^2 / \hat{r}_{\rm max}^2. \tag{45}$$

Using angular distributions of the radiation field in the far diffraction zone we can trace the dependence of the degree of transverse coherence versus undulator length. Solid line in Fig. 9 is the result of analytical calculations, and the circles are the results obtained with numerical simulation code. We can state that there is good agreement between analytical and simulation results. It is clearly seen that the degree of coherence differs visibly from the unity in the high-gain linear regime, $\zeta \simeq 0.9$ at $\hat{z} = 15$.

Another possible way to define the degree of coherence is based on the statistical analysis of fluctuations of the instantaneous power. Since in the linear regime we deal with a Gaussian random process, the power density at fixed point in space fluctuates in accordance with the negative exponential distribution [21]. If there is full transverse coherence then the same refers to the instantaneous power W equal to the power density integrated over cross-section of the radiation pulse. If the radiation is partially coherent, then we have a more general law for instantaneous power fluctuations, namely the gamma distribution [21,22]:

$$p(W) = \frac{M^M}{\Gamma(M)} \left(\frac{W}{\langle W \rangle} \right)^{M-1} \frac{1}{\langle W \rangle} \exp\left(- M \frac{W}{\langle W \rangle} \right), \tag{46}$$

where $\Gamma(M)$ is the gamma function with argument M, and

$$M = \frac{1}{\sigma_W^2}, \quad \sigma_W^2 = \langle (W - \langle W \rangle)^2 \rangle / \langle W \rangle^2. \tag{47}$$

The parameter $M = 1/\sigma_W^2$ of this distribution can be considered as the number of transverse modes. Then the degree of coherence in the linear regime, ζ, may be defined as follows

$$\zeta = \frac{1}{M} = \sigma_W^2. \tag{48}$$

The value of M should be calculated with numerical simulation code producing time-dependent results for the radiation power (see Fig. 2). Fig. 10 presents the probability distribution of the fluctuations of the radiation power for two different undulator lengths of $\hat{z} = 8$ and $\hat{z} = 15$. In Fig. 11 we present the dependence of the number of transverse modes on the undulator length for the specific value $B = 1$ of the diffraction parameter. It is seen that both definitions for the degree for the transverse coherence, Eqs. (45) and (48), are consistent in the high-gain linear regime.

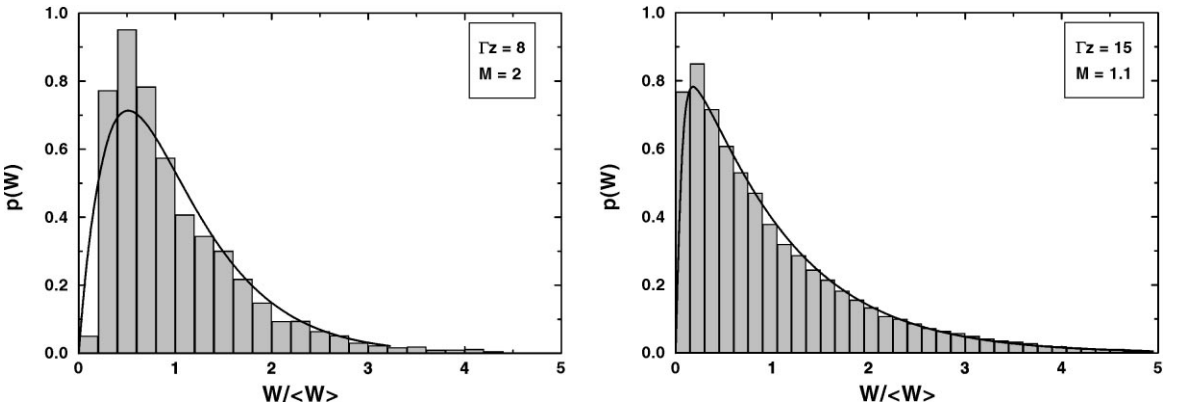


Fig. 10. Histogram of the probability distribution of the instantaneous radiation power from the FEL amplifier starting from shot noise at the length of undulator of $\hat{z} = 8$ (left plot) and $\hat{z} = 15$ (right plot). Here $B = 1$, $\Lambda_{\mathrm{p}}^2 \to 0$, $\Lambda_T^2 = 0$, and $\hat{z} = 8$. Calculations have been performed with linear simulation code FAST. Solid lines represents gamma distribution with $M = 2$ (left plot) an $M = 1.1$ (right plot).

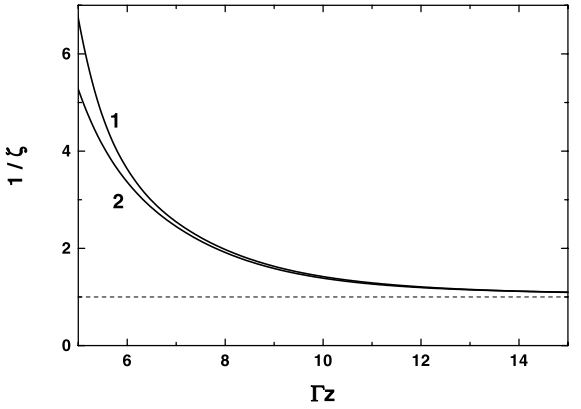


Fig. 11. Inverse value of transverse coherence versus undulator length. Here $B = 1$, $\Lambda_{\mathrm{p}}^2 \to 0$, $\Lambda_T^2 = 0$, and $N_{\mathrm{c}} = 7 \times 10^7$. Calculations have been performed with linear simulation code FAST. Curve 1 is calculated using instantaneous fluctuations of the radiation power (48). Curve 2 is calculated with Eq. (45).

7. Discussion

Let us discuss asymptotical behavior of the degree of transverse coherence. At a large value of the undulator length it approaches to unity asymptotically as $(1 - \zeta) \propto 1/z$, but not exponentially, as one can expect from simple physical assumption that transverse coherence establishes due to the transverse mode selection. The latter effect indeed takes place as it is illustrated in Fig. 1. That is why the degree of coherence grows quickly at an early stage of amplification. Starting from some undulator length the contribution to the total power of the fundamental mode becomes to be dominant (see Fig. 4). However, one should take into account that the spectrum width has always finite value (see Fig. 8). Actually this means that in the high-gain linear regime the radiation of the SASE FEL is formed by many fundamental TEM_{00} modes with different frequencies. The transverse distribution of the radiation field of the mode is also different for

different frequencies. As a result of interference of these modes we do not have full transverse coherence. Taking into account this consideration, we can simply explain asymptotical behavior of the degree of transverse coherence – this is reflection of the slow evolution of the width of the radiation spectrum as $z^{-1/2}$ with the undulator length.

All the results presented above have been obtained in the framework of the linear theory. Simulations with nonlinear code shows that for the considered numerical example the saturation occurs at $\hat{z} \simeq 18$. Using the plot presented in Fig. 9 we find that the value of the transverse coherence is less than 0.9 in the end of the linear regime. A typical range of the values of N_c is 10^6–10^9 for the SASE FEL of wavelength range from X-ray up to infrared. The numerical example presented in this paper is calculated for $N_c = 7 \times 10^7$ which is typical for a VUV FEL. It is worth to mention that the dependence of the saturation length of the SASE FEL on the value of N_c is rather weak, in fact logarithmic (see Eq. (33)). Therefore, we can state that obtained effect limiting the value of transverse coherence might be important for practical SASE FELs.

References

[1] W.M. Fawley, An Informal Manual for GINGER and its Post-processor XPLOTGIN", LBID-2141, CBT Tech Note-104, UC-414, 1995.
[2] S. Reiche, Nucl. Instrum. Meth. A 429 (1999) 243.
[3] E.L. Saldin, E.A. Schneidmiller, M.V. Yurkov, Nucl. Instrum. Meth. A 429 (1999) 233.
[4] A VUV Free Electron Laser at the TESLA Test Facility: Conceptual Design Report, DESY Print TESLA-FEL 95-03, Hamburg, DESY, 1995.
[5] J. Rossbach, Nucl. Instrum. Meth. A 375 (1996) 269.
[6] R. Brinkmann, et al. (Eds.), Conceptual Design of 500 GeV e^+ e^- Linear Collider with Integrated X-ray Facility, DESY 1997-048, ECFA 1997-182, Hamburg, May 1997.
[7] Linac Coherent Light Source (LCLS) Design Study Report, The LCLS Design Study Group, Stanford Linear Accelerator Center (SLAC) Report no. SLAC-R-521, 1998.
[8] K.J. Kim, Nucl. Instrum. Meth. A 250 (1986) 396.
[9] J.M. Wang, L.H. Yu, Nucl. Instrum. Meth. A 250 (1986) 484.
[10] W.B. Colson, in: W.B. Colson, et al. (Eds.), Laser Handbook, vol. 6: Free Electron Laser, North-Holland, Amsterdam, 1990, p. 115.
[11] R. Bonifacio, et al., Phys. Rev. Lett. 73 (1994) 70.
[12] P. Pierini, W. Fawley, Nucl. Instrum. Meth. A 375 (1996) 332.
[13] E.L. Saldin, E.A. Schneidmiller, M.V. Yurkov, Nucl. Instrum. Meth. A 393 (1997) 157.
[14] E.L. Saldin, E.A. Schneidmiller, M.V. Yurkov, Opt. Commun. 148 (1998) 383.
[15] G.T. Moore, Opt. Commun. 52 (1984) 46.
[16] G.T. Moore, Nucl. Instrum. Meth. A 250 (1986) 381.
[17] K.J. Kim, Phys. Rev. Lett. 57 (1986) 1871.
[18] N.G. van Kampen, Physica 21 (1951) 949.
[19] S. Krinsky, L.H. Yu, Phys. Rev. A 35 (1987) 3406.
[20] E.L. Saldin, E.A. Schneidmiller, M.V. Yurkov, Opt. Commun. 97 (1993) 272.
[21] E.L. Saldin, E.A. Schneidmiller, M.V. Yurkov, The Physics of Free Electron Laser, Springer, Berlin, 1999.
[22] E.L. Saldin, E.A. Schneidmiller, M.V. Yurkov, Nucl. Instrum. Meth. A 429 (1999) 229.